

线黏弹性端接布拉格光纤光栅传感器应变传递机理

陈光^{1,2*}, 丁克勤¹, 冯其波², 高瞻²¹中国特种设备检测研究院, 北京 100029;²北京交通大学理学院, 北京 100044

摘要 端接光纤光栅应变传感器具有无多峰、栅区不直接受力和各点受力相等等优点,在基片式和夹持式等传感器封装中得到广泛应用。但黏接层的剪切变形会导致光纤光栅测量应变与基体结构应变不同,从而产生应变测量误差。实际使用中,需要准确获得黏接层剪切变形影响下光纤光栅应变与基体结构应变的函数关系,以提高应变的测量精度。为此,推导了线黏弹性表面黏贴式端接光纤光栅应变传递方程,建立了瞬时响应和准静态响应下光纤光栅和基体之间的平均应变传递模型。讨论分析了影响平均应变传递率的因素,给出明显优于栅区黏接式光纤光栅应变传感器的黏接层参数的影响规律。通过有限元仿真验证了理论方程的有效性。该模型为端接光纤光栅应变传感器的设计与应用提供依据。

关键词 光纤光学; 应变传递; 端接光纤光栅; 光纤传感; 表面黏贴; 线黏弹性

中图分类号 TN253

文献标识码 A

doi: 10.3788/LOP55.110604

Strain Transfer Mechanism of End-Bonding Fibre Bragg Grating Sensors Based on Linear Viscoelasticity

Chen Guang^{1,2*}, Ding Keqin¹, Feng Qibo², Gao Zhan²¹China Special Equipment Inspection and Research Institute, Beijing 100029, China;²School of Science, Beijing Jiaotong University, Beijing 100044, China

Abstract The end-bonding fiber Bragg grating (FBG) sensors have many advantages such as no multiple peaks, no direct force in grating area and all points suffering the same stress, which are widely used to the packaging of substrate-type, clamp-type and other types of sensors. However, the shear deformation in the adhesive layer results in the difference between FBG strain and matrix strain, and thus the strain measurement error is introduced. In the practical applications, it is necessary to precisely obtain the function relationship between the FBG strain and the matrix strain under the influence of the shear deformation in the adhesive layer to improve the measurement accuracy of strain. For this purpose, the strain transfer equation of end-bonding FBGs based on linear viscoelasticity is derived and the average strain transfer models between fiber grating and matrix under instantaneous response and quasi-static response are developed. The parameters that influence the average strain transfer rate are discussed and analyzed. The influence law of the adhesive layer parameters with which the grating is obviously superior to that of a grating-bonding FBG sensor is demonstrated. The validity of the theoretical equation is verified by the simulation by the finite element method, and the proposed model provides a theoretical basis for the design and application of end-bonding FBG strain sensors.

Key words fiber optics; strain transfer; end-bonding fiber Bragg grating; optical fiber sensing; surface adhesion; linear viscoelasticity

OCIS codes 060.2370; 060.2310; 060.2300

1 引言

光纤光栅传感器(FBG)由于具有质量小、体积

小、抗电磁干扰能力强、灵敏度高和易于复用等优点,在结构损伤监测领域中得到了广泛应用。当光纤光栅应用于基体结构的应力应变监测时,由于光

收稿日期: 2018-04-24; 修回日期: 2018-05-18; 录用日期: 2018-06-06

基金项目: 国家 863 计划(2015AA043702)

* E-mail: chenguang015@163.com

纤光栅和基体结构通过中间层固定,存在应变传递损耗,因此光纤光栅所测得的应变与基体的应变不同^[1]。国内外科研工作者开展了大量针对光纤应变与基体应变之间关系的研究,取得了大量成果。Ansari 等^[2-11]采用一定的假设条件,得出埋入式光纤光栅应变传感器的传递表达式。Qin 等^[12-19]推导出表面黏贴式光纤光栅传感器的应变传递方程。刘明尧等^[20-21]推导了胶层黏弹性的表面黏贴式和埋入式 FBG 传感器的应变传递规律。但是,上述研究均是针对栅区黏贴光纤光栅传感器的应变传递。尽管栅区黏接工艺简便,但栅区黏接传感器中胶黏性和受力的不确定性易产生多峰现象,从而导致结果的错误判断。与栅区黏接相比,端接黏接的传感器仅 FBG 栅区两端受力,栅区不直接受力,栅区内各点受力相等。吴俊等^[22]依据变形等效原理,推导了表面黏贴式非栅区封装 FBG 的应变传递函数,但是推导中仅考虑了黏接层弹性模量和栅区长度的影响。Sun 等^[23]基于对称性推导了夹持式光纤光栅传感器的应变传递公式。

本文推导了线黏弹性表面端接黏贴式光纤光栅与基体结构之间的应变传递关系,讨论分析了影响平均应变传递率的因素,通过有限元验证了理论方程的有效性。

2 线黏弹性表面黏贴式端接光纤光栅传感器应变传递机理

表面黏贴式端接 FBG 传感器主要由基体、FBG (光纤纤芯和包层) 和黏接层组成,表面黏贴式端接 FBG 传感器示意图如图 1 所示。其中, L 为单侧黏接层长度, L_f 为栅区长度。将 FBG 两端去除涂覆层,在施加预应力条件下将其用黏结剂粘贴在基体结构上。其应变传递过程为:基体结构在外部荷载作用下产生应变,在剪应力的作用下,基体结构应变传递给黏接层进而传递给光纤,使光纤产生轴向应变,光纤两端带动光栅栅区产生轴向应变,进而改变 FBG 的反射波长。裸 FBG 粘贴于基体表面时的侧视图如图 2 所示, D , H 和 h 分别表示黏接层宽度、黏接高度和黏接层下表面到光纤下表面的距离(简称下部厚度)。

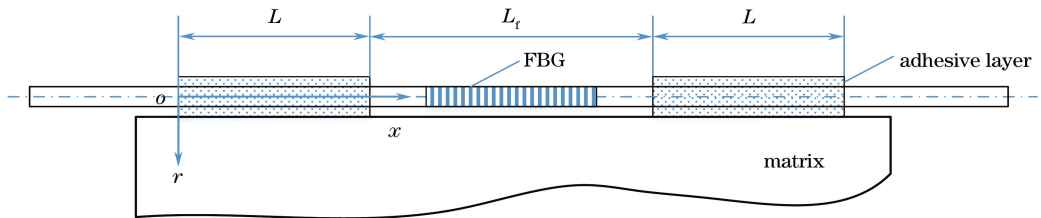


图 1 表面黏贴式端接 FBG 传感器示意图

Fig. 1 Schematic of surface adhesive and end-bonding FBG sensor

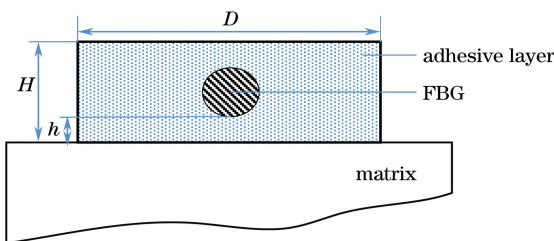


图 2 裸 FBG 粘贴于基体表面时的侧视图

Fig. 2 Side view of bare FBG bonded on matrix surface

为简化分析模型,采用如下假设:光纤、黏接层和基体之间交界面结合紧密,没有脱落;光纤和基体结构均为线弹性材料,并且基体沿光纤的轴线方向均匀变形;黏接层为线黏弹性材料;只有基体结构受到轴向外力作用时,其应变通过剪应变传递,而黏贴层和光纤不直接受力;不考虑温度等环境的影响。

图 3 为剪切力传递示意图。其中, σ 和 ϵ 分别表示轴向应力和轴向应变; τ 和 γ 分别表示剪切应力和剪切应变;下标 g, a 和 m 分别代表光纤、黏接

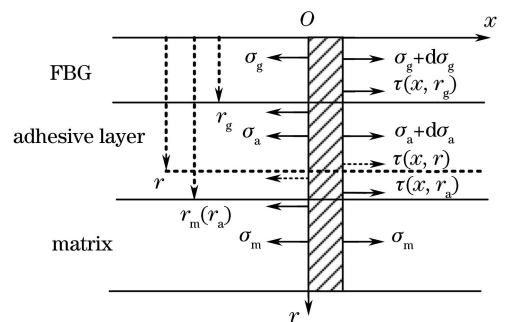


图 3 剪切力传递示意图

Fig. 3 Schematic of strain transfer

层和基体的物理量(下同); r 为表示坐标中到光纤中心的空变量。

沿 x 方向对纤芯微元段进行受力分析,可得

$$\tau_g(x, r_g, t) = -\frac{r_g}{2} \frac{d\sigma_g(x, t)}{dx}. \quad (1)$$

对黏接层微段进行受力分析,可得

$$\tau_a(x, r, t) = - \frac{[D(H - r_g - h + r) - \pi r_g^2] \left[\frac{d\sigma_a(x, t)}{dx} \right] + \pi r_g^2 \left[\frac{d\sigma_g(x, t)}{dx} \right]}{D}, \quad r_g < r < r_a. \quad (2)$$

根据材料黏弹性积分型本构方程, 可得黏接层应力/应变关系的 Stieltjes 卷积缩写形式, 即

$$\gamma(x, r, t) = X(t) * d\tau(x, r, t), \quad (3)$$

$$\varepsilon(x, t) = B(t) * d\sigma(x, t), \quad (4)$$

式中: $X(t)$ 和 $B(t)$ 分别为剪切蠕变柔量和拉压蠕变柔量; * 代表卷积。

对(2)式和(4)式进行拉普拉斯(Laplace)变换, 可得

$$\bar{\tau}_a(x, r, s) = - \frac{[D(H - r_g - h + r) - \pi r_g^2] \left[\frac{d\bar{\sigma}_a(x, s)}{dx} \right] + \pi r_g^2 \left[\frac{d\bar{\sigma}_g(x, s)}{dx} \right]}{D}, \quad (5)$$

$$\bar{\tau}_a(x, r, s) = - \frac{[D(H - r_g - h + r) - \pi r_g^2]}{D} \frac{1}{\bar{B}_a(s) \cdot s} \frac{d\bar{\varepsilon}_a(x, s)}{dx} - \frac{\pi r_g^2}{D} \frac{1}{\bar{B}_g(s) \cdot s} \frac{d\bar{\varepsilon}_g(x, s)}{dx}, \quad (6)$$

式中: s 为复变量。对(3)式进行 Laplace 变换, 可得

$$\bar{\gamma}_a(x, r, s) = - \frac{[D(H - r_g - h + r) - \pi r_g^2]}{D} \frac{\bar{X}_a(s)}{\bar{B}_a(s)} \frac{d\bar{\varepsilon}_a(x, s)}{dx} - \frac{\pi r_g^2}{D} \frac{\bar{X}_a(s)}{\bar{B}_g(s)} \frac{d\bar{\varepsilon}_g(x, s)}{dx}. \quad (7)$$

根据积分型本构方程弹性-黏弹性对应原理, 可得

$$\bar{X}_a(s) = 2 \bar{B}_a(s) [1 + \nu_a(s) \cdot s], \quad (8)$$

式中: $\nu_a(s)$ 为黏接层的泊松比。

$$\begin{aligned} \bar{\gamma}_a(x, r, s) = & -2 [1 + \nu_a(s) \cdot s] \cdot \\ & \frac{[D(H - r_g - h + r) - \pi r_g^2]}{D} \frac{d\bar{\varepsilon}_a(x, s)}{dx} - \\ & 2 [1 + \nu_a(s) \cdot s] \frac{\pi r_g^2}{D} \frac{\bar{B}_a(s)}{\bar{B}_g(s)} \frac{d\bar{\varepsilon}_g(x, s)}{dx}. \end{aligned} \quad (9)$$

中间层一般为环氧树脂胶, 其蠕变柔量与光纤相差较大(一般 10 倍以上), 故可认为

$$\begin{aligned} \frac{[D(H - r_g - h + r) - \pi r_g^2]}{D} \frac{d\bar{\varepsilon}_a}{dx} = \\ O\left(\frac{d\bar{\varepsilon}_g}{dx}\right), \end{aligned} \quad (10)$$

$$\begin{aligned} \bar{\gamma}_a(x, r, s) = \\ -2 [1 + \nu_a(s) \cdot s] \frac{\pi r_g^2}{D} \frac{\bar{B}_a(s)}{\bar{B}_g(s)} \frac{d\bar{\varepsilon}_g(x, s)}{dx}. \end{aligned} \quad (11)$$

由于光纤的长度远大于其直径, 因此忽略光纤径向变形, 可得

$$\tau(x, r) = G_a \gamma_a(x, r) = G_a \left(\frac{\partial u}{\partial r} + \frac{\partial v}{\partial r} \right) \simeq G_a \frac{du}{dr}, \quad (12)$$

式中: G 为剪切模量。仅考虑轴向变形, 则对(11)式积分可得非栅区黏接层内侧受力为

$$u_m(x, t) - u_g(x, t) = \int_{r_g}^{r_g+h} \gamma_a(x, r, t) dr. \quad (13)$$

对(13)式两边进行 Laplace 变换, 可得

$$\begin{aligned} \bar{u}_m(x, s) - \bar{u}_g(x, s) = \\ \int_{r_g}^{r_g+h} \bar{\gamma}_a(x, r, s) dr = -2 [1 + \nu_a(s) \cdot s] \cdot \\ h \frac{\pi r_g^2}{D} \frac{\bar{B}_a(s)}{\bar{B}_g(s)} \frac{d\bar{\varepsilon}_g(x, s)}{dx}. \end{aligned} \quad (14)$$

令

$$\bar{k}^2 = \left\{ 2 [1 + \nu_a(s) \cdot s] h \frac{\pi r_g^2}{D} \frac{\bar{B}_a(s)}{\bar{B}_g(s)} \right\}^{-1}, \quad (15)$$

对 x 求导得

$$\begin{aligned} \frac{d^2 \bar{\varepsilon}_g(x, s)}{dx^2} - \bar{k}^2 \bar{\varepsilon}_g(x, s) + \\ \bar{k}^2 \bar{\varepsilon}_m(x, s) = 0, \end{aligned} \quad (16)$$

其通解为

$$\begin{aligned} \bar{\varepsilon}_g(x, s) = c_1 \exp(\bar{k}x) + \\ c_2 \exp(-\bar{k}x) + \bar{\varepsilon}_m(x, s), \end{aligned} \quad (17)$$

式中: c_1 和 c_2 由边界条件决定。光纤的一端为自由端, 没有应力传递; 光纤另一端近似为 FBG 的实测应变 ε_f 。则边界条件为

$$\begin{cases} \varepsilon_g(0, t) = 0 \\ \varepsilon_g(L, t) = \varepsilon_f \end{cases}, \quad (18)$$

经 Laplace 变换得

$$\begin{cases} \bar{\varepsilon}_g(0, s) = 0 \\ \bar{\varepsilon}_g(L, s) = \bar{\varepsilon}_f \end{cases}, \quad (19)$$

代入(17)式可得

$$\begin{cases} c_1 = \frac{\bar{\epsilon}_f + [\exp(-\bar{k}L) - 1] \bar{\epsilon}_m(x, s)}{2\sinh(\bar{k}L)} \\ c_2 = -\frac{\bar{\epsilon}_f + [\exp(\bar{k}L) - 1] \bar{\epsilon}_m(x, s)}{2\sinh(\bar{k}L)} \end{cases} \quad (20)$$

所以黏接区域光纤应变方程为

$$\bar{\epsilon}_g(x, s) = \frac{\bar{\epsilon}_f + [\exp(-\bar{k}L) - 1] \bar{\epsilon}_m(x, s)}{2\sinh(\bar{k}L)} \cdot \exp(\bar{k}x) - \frac{\bar{\epsilon}_f + [\exp(\bar{k}L) - 1] \bar{\epsilon}_m(x, s)}{2\sinh(\bar{k}L)}.$$

$$\exp(-\bar{k}x) + \bar{\epsilon}_m(x, s). \quad (21)$$

根据图 1, 光纤实测应变和基体结构的应变可表示为

$$\bar{\epsilon}_f = \frac{\Delta L_f}{L_f}, \quad (22)$$

$$\bar{\epsilon}_m(x, s) = \frac{\Delta L_f + 2\Delta L}{L_f + 2L}. \quad (23)$$

根据光纤、黏贴层和基体结构同步变形, 光纤轴向变化量与基体轴向变化量相同, 可得

$$\Delta L = \int_0^L \bar{\epsilon}_g(x, s) dx = \int_0^L \left\{ \frac{\bar{\epsilon}_f + [\exp(-\bar{k}L) - 1] \bar{\epsilon}_m(x, s)}{2\sinh(\bar{k}L)} \exp(\bar{k}x) - \frac{\bar{\epsilon}_f + [\exp(\bar{k}L) - 1] \bar{\epsilon}_m(x, s)}{2\sinh(\bar{k}L)} \exp(-\bar{k}x) + \bar{\epsilon}_m(x, s) \right\} dx = \frac{\bar{\epsilon}_m(x, s) [2\bar{k}^2 - 2(\bar{k}^2 + 1)\cosh(\bar{k}L) + 2\bar{k}L\sinh(\bar{k}L)] + \bar{\epsilon}_f [\bar{k}^2 \exp(\bar{k}L) - \bar{k}^2 + \exp(-\bar{k}L) - 1]}{2\bar{k}\sinh(\bar{k}L)}. \quad (24)$$

在基体受到 $\sigma(t) = \sigma_0 H(t)$ 作用下时, 由(21)~(24)式得, 光纤测量应变与基体的平均应变传递率为

$$\bar{\alpha}(x, t) = \frac{\epsilon_f}{\epsilon_m} = \mathcal{L}^{-1} \left\{ \frac{1}{s} \cdot \frac{2(\bar{k}^2 + 1) - \bar{k}L_f \sinh(\bar{k}L) - (2\bar{k}^2 + 1)\cosh(\bar{k}L)}{1 - \bar{k}L_f \sinh(\bar{k}L) + \bar{k}^2 [\exp(\bar{k}L) - 1] - \exp(-\bar{k}L)} \right\}, \quad (25)$$

式中: \mathcal{L}^{-1} 为 Laplace 逆变换; $H(t)$ 为 Heavside 函数, 定义为

$$H(t) = \begin{cases} 1, & t \geq 0 \\ 0, & t < 0 \end{cases} \quad (26)$$

3 瞬时和准静态应变传递分析

将黏贴层的黏弹性模型简化为一个 Kelvin 模型和一个弹簧串联而成的标准线性固体模型, 如图 4 所示。

标准线性固体模型在应力 $\sigma(t) = \sigma_0 H(t)$ 的作用下, 有

$$B_a(t) = \frac{1}{E_{a2}} + \frac{1}{E_{a1}} \left[1 - \exp\left(-\frac{t}{\tau}\right) \right]. \quad (27)$$

式中: $\tau = \eta_1 / E_{a1}$ 为松弛时间; E 为杨氏模量。

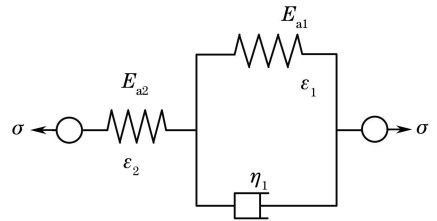


图 4 标准线性固体模型

Fig. 4 Standard linear solid model

瞬时蠕变柔量为

$$B_a(0^+) = \lim_{s \rightarrow \infty} s \cdot \bar{B}_a(s) = \frac{1}{E_{a2}}. \quad (28)$$

准静态蠕变柔量为

$$B_a(\infty) = \lim_{s \rightarrow 0^+} s \cdot \bar{B}_a(s) = \frac{E_{a2} + E_{a1}}{E_{a2} E_{a1}}. \quad (29)$$

则可得 FBG 瞬时响应为

$$\lim_{s \rightarrow \infty} \bar{k} = \left\{ 2 [1 + \nu_a(s) \cdot s] (r_a - r_g) \frac{\pi r_g^2 \bar{B}_a(0^+)}{D \bar{B}_g(0^+)} \right\}^{-1/2} = k_0, \quad (30)$$

$$\bar{\alpha}(0^+) = \frac{\bar{\epsilon}_f}{\bar{\epsilon}_m(x, 0^+)} = \frac{2(k_0^2 + 1) - k_0 L_f \sinh(k_0 L) - (2k_0^2 + 1)\cosh(k_0 L)}{1 - k_0 L_f \sinh(k_0 L) + k_0^2 [\exp(k_0 L) - 1] - \exp(-k_0 L)}. \quad (31)$$

准静态的应变传递率为

$$\lim_{s \rightarrow 0^+} \bar{k} = \left[2 [1 + \nu_a(s) \cdot s] (r_a - r_g) \frac{\pi r_g^2 \bar{B}_a(\infty)}{D \bar{B}_g(\infty)} \right]^{-1/2} = k_\infty, \quad (32)$$

$$\bar{\alpha}(\infty) = \frac{\bar{\epsilon}_f}{\epsilon_m(x, \infty)} = \frac{2(k_\infty^2 + 1) - k_\infty L_f \sinh(k_\infty L) - (2k_\infty^2 + 1) \cosh(k_\infty L)}{1 - k_\infty L_f \sinh(k_\infty L) + k_\infty^2 [\exp(k_\infty L) - 1] - \exp(-k_\infty L)}. \quad (33)$$

4 分析与讨论

4.1 黏接层参数影响分析

光纤和黏接层的物理参数如表 1 和表 2 所示,黏接层物理参数初值设定为 $E_a = 4 \times 10^9$ Pa, $\nu = 0.34$, $h = 0.1$ mm, $D = 4$ mm, $L = 2$ mm, $L_f = 20$ mm。图 5 为黏接层参数对线黏弹性端接 FBG 黏贴平均应变传递率的影响。

表 1 光纤的物理参数

Table 1 Physical parameters of optical fiber

Material parameter	Value
Young's modulus $E_g / (10^{10}$ Pa)	7.2
Radius r_g / nm	62.5

由图 5(a)~(d) 可见,平均应变传递率均随黏接层长度、宽度和杨氏模量的增加而增加,随黏接层

下部厚度和泊松比的增加而减小,瞬时响应值均大于准静态响应值。由图 5(a)~(c) 可见,在黏接层物理参数的初设值下,在 $L \geq 0.5$ mm、 $D > 0.2$ mm 和 $E_a > 0.3 \times 10^9$ Pa 时,瞬时响应值和准静态响应值相差小于 5%;图 5(d) 中随黏接层下部厚度的增加,在 0.1~2 mm 内瞬时响应值和准静态响应值相差小于 5%。

表 2 黏接层的物理参数

Table 2 Physical parameters of adhesive layer

Material parameter	Value
Poisson's ratio ν	0.24-0.44
Young's modulus $E_a / (10^9$ Pa)	0.05-4.00
Single bonding length L / mm	0.1-2.0
Bonding width D / mm	0.5-4.0
Bonding height H / mm	0-2.5
Lower thickness h / mm	0.1-2.0

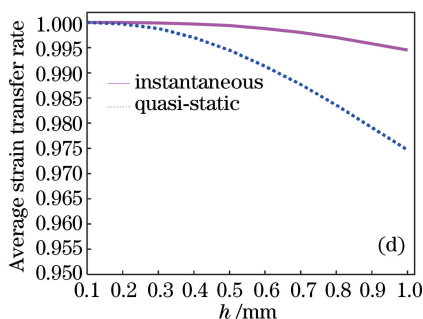
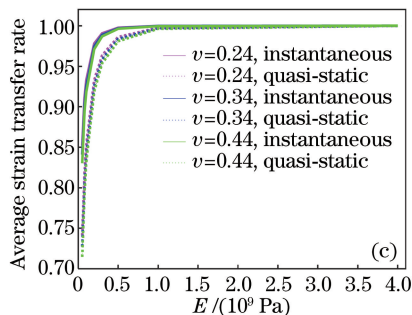
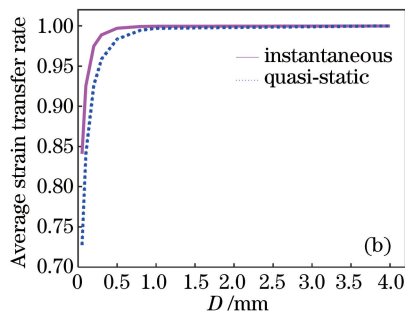
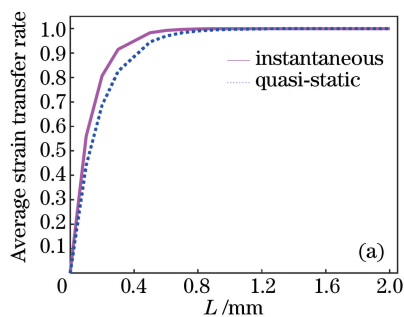


图 5 黏接层参数对应变传递率的影响。(a)长度;(b)宽度;(c)杨氏模量;(d)下部厚度

Fig. 5 Influences of adhesive layer parameters on strain transfer rate. (a) Length; (b) width; (c) Young's modulus; (d) thickness of lower part

4.2 数值验证

为验证理论预测模型的有效性,利用 ANSYS Workbench 17.0 进行有限元(FEM)分析。黏接层参数: $E_a = 4 \times 10^9$ Pa, $\nu = 0.34$, $H = 0.2425$ mm, $h =$

0.1 mm, $D = 4$ mm, $L = 0.1 \sim 2.0$ mm, 基体结构的长×宽×高为 0.03 m×0.02 m×0.01 m, $G_m = 7.7 \times 10^{10}$ Pa。

图 6 为有限元网格划分。图 7 为理论解和有限

元结果对比。由图 7 可见,瞬时情况下 FBG 平均应变传递率和有限元分析在单侧黏结长度的分布趋势是相同的,且理论解略大于数值解。

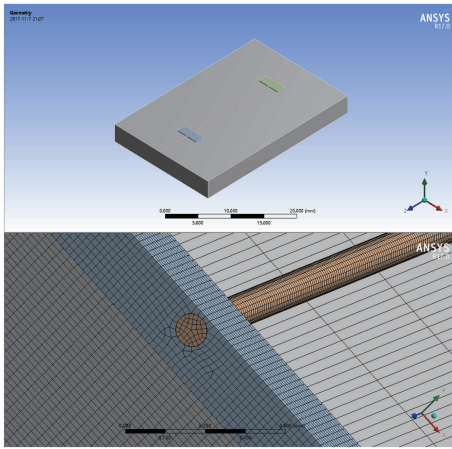


图 6 有限元网格划分

Fig. 6 Finite element meshes

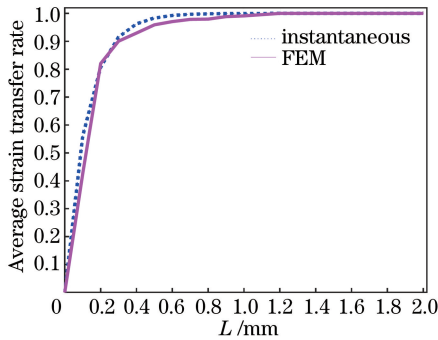


图 7 理论解和有限元结果对比

Fig. 7 Comparison between theoretical solutions and results obtained by FEM

5 结 论

端接光纤光栅应变传感器已经得到越来越广泛的应用。以表面端接黏贴式光纤光栅为研究对象,基于剪滞理论,研究了表面黏贴式端接光纤光栅应变传递机理,建立了光纤光栅和基体之间的平均应变传递模型,给出表面黏贴式端接光纤光栅传感器的参数优化规律。与现有的方法相比,本方法提高了测量精度,简化了封装工艺。为了验证理论预测的正确性,利用有限元法与提出的模型进行对比,结果表明两者具有很好的一致性。提出的模型为端接光纤光栅应变传感器的设计和应用提供了理论依据。

参 考 文 献

[1] Cheng C C, Lo Y, Li W Y. Accurate simulations of reflective wavelength spectrum of surface-bonded

fiber Bragg grating [J]. Applied Optics, 2010, 49 (17): 3394-3402.

- [2] Ansari F, Yuan L B. Mechanics of bond and interface shear transfer in optical fiber sensors [J]. Journal of Engineering Mechanics, 1998, 124(4): 385-394.
- [3] Lau K T, Yuan L B, Zhou L M, *et al.* Strain monitoring in FRP laminates and concrete beams using FBG sensors [J]. Composite Structures, 2001, 51(1): 9-20.
- [4] Li D S, Li H N, Ren L, *et al.* Strain transferring analysis of fiber Bragg grating sensors [J]. Optical Engineering, 2006, 45(2): 024402.
- [5] Li Q B, Li G, Wang G L, *et al.* Elasto-plastic bonding of embedded optical fiber sensors in concrete [J]. Journal of Engineering Mechanics, 2002, 128 (4): 471-478.
- [6] Zhou J, Zhou Z, Zhang D. Study on strain transfer characteristics of fiber Bragg grating sensors [J]. Journal of Intelligent Material Systems and Structures, 2010, 21(11): 1117-1122.
- [7] Wang H P, Zhou Z. Advances of strain transfer analysis of optical fibre sensors [J]. Pacific Science Review, 2014, 16(1): 8-18.
- [8] Li H N, Zhou G D, Ren L, *et al.* Strain transfer coefficient analyses for embedded fiber Bragg grating sensors in different host materials [J]. Journal of Engineering Mechanics, 2009, 135(12): 1343-1353.
- [9] Wu R J, Zheng B L, Fu K K, *et al.* Study on strain transfer of embedded fiber Bragg grating sensors [J]. Optical Engineering, 2014, 53(8): 085105.
- [10] Wan K T, Leung C K Y, Olson N G. Investigation of the strain transfer for surface-attached optical fiber strain sensors [J]. Smart Materials and Structures, 2008, 17(3): 035037.
- [11] Qin H Y, Zhu W X, Zhang H L, *et al.* Manufacturing and performance analysis of intelligent steel strand embedded with prepressure large scale fiber Bragg grating sensor [J]. Chinese Journal of Lasers, 2017, 44(4): 0410001.
覃荷瑛, 朱万旭, 张贺雨, 等. 内嵌预压式大量程光纤光栅传感器的智能钢绞线的研制与性能分析 [J]. 中国激光, 2017, 44(4): 0410001.
- [12] Qin H Y, Huo T T, Zhu W X. Desensitization effect of helix-slant composite technology on fiber Bragg grating sensor [J]. Laser & Optoelectronics Progress, 2017, 54(3): 030601.
覃荷瑛, 霍婷婷, 朱万旭. 螺旋倾斜复合技术对光纤布拉格光栅传感器的减敏作用 [J]. 激光与光电子学

- 进展, 2017, 54(3): 030601.
- [13] Wan K T. Quantitative sensitivity analysis of surface attached optical fiber strain sensor[J]. IEEE Sensors Journal, 2014, 14(6): 1805-1812.
- [14] Her S C, Huang C Y. Effect of coating on the strain transfer of optical fiber sensors[J]. Sensors, 2011, 11(7): 6926-6941.
- [15] Wang Q B, Qiu Y, Zhao H T, *et al.* Analysis of strain transfer of six-layer surface-bonded fiber Bragg gratings[J]. Applied Optics, 2012, 51(18): 4129-4138.
- [16] Zhao H T, Wang Q B, Qiu Y, *et al.* Strain transfer of surface-bonded fiber Bragg grating sensors for airship envelope structural health monitoring [J]. Journal of Zhejiang University SCIENCE A, 2012, 13(7): 538-545.
- [17] Tian S Z, Zhang G Q, Wang D P. Study on strain transfer mechanism of surface fiber Bragg grating sensor[J]. Chinese Journal of Lasers, 2014, 41(8): 0805005.
田石柱, 张国庆, 王大鹏. 表面式光纤布拉格光栅传感器应变传递机理的研究[J]. 中国激光, 2014, 41(8): 0805005.
- [18] Zhang G H, Chai J, Li X J, *et al.* Research on strain transfer of surface fiber grating sensor[J]. Laser & Optoelectronics Progress, 2014, 51(1): 010601.
张桂花, 柴敬, 李旭娟, 等. 基片式光纤光栅应变传感器的应变传递研究[J]. 激光与光电子学进展, 2014, 51(1): 010601.
- [19] You Z W, Wang Y, Sun Y Y, *et al.* Experimental research on strain transfer rules of prestressing fiber Bragg grating[J]. Laser & Optoelectronics Progress, 2016, 53(11): 110501.
由泽伟, 王源, 孙阳阳, 等. 预张拉光纤布拉格光栅应变传递规律实验研究[J]. 激光与光电子学进展, 2016, 53(11): 110501.
- [20] Liu M Y, Ji D L, Xiao S, *et al.* Effect of adhesive viscoelasticity on strain transfer mechanism of bonded FBG[J]. Optics and Precision Engineering, 2016, 24(6): 1307-1318.
刘明尧, 季冬亮, 肖爽, 等. 胶黏剂黏弹性对黏贴式FBG应变传递的影响[J]. 光学精密工程, 2016, 24(6): 1307-1318.
- [21] Chang X L, Li M, Gu X F. Research on strain transfer of embedded polymer optical fiber sensors based on linear viscoelasticity [J]. Journal of Solid Rocket Technology, 2010, 33(3): 353-359.
常新龙, 李明, 谷小飞. 基于线黏弹性的埋入式聚合物光纤传感器应变传递研究[J]. 固体火箭技术, 2010, 33(3): 353-359.
- [22] Wu J, Chen W M, Yu K, *et al.* Strain sensing properties of grating ends packaged FBG sensors[J]. Acta Photonica Sinica, 2016, 45(2): 0206004.
吴俊, 陈伟民, 余葵, 等. 非栅区封装光纤布喇格光栅应变传感特性研究[J]. 光子学报, 2016, 45(2): 0206004.
- [23] Sun L, Li C, Li J, *et al.* Strain transfer analysis of a clamped fiber Bragg grating sensor [J]. Applied Sciences, 2017, 7(2): 188.